Geologos 20, 4 (2014): 289–301
10.2478/logos-2014-0017

GEOLOGOS

Identification and visualisation of possible ancient ocean shoreline on Mars using submeter-resolution Digital Terrain Models

Andrzej Świąder

Faculty of Geology, Geophysics and Environmental Protection, AGH University of Science and Technology, Mickiewicza 30, 30-059 Kraków, Poland;
e-mail: andrzej.swiader@agh.edu.pl

Abstract

Digital Terrain Models (DTMs) produced from stereoscopic, submeter-resolution High Resolution Imaging Science Experiment (HiRISE) imagery provide a solid basis for all morphometric analyses of the surface of Mars. In view of the fact that a more effective use of DTMs is hindered by complicated and time-consuming manual handling, the automated process provided by specialists of the Ames Intelligent Robotics Group (NASA), Ames Stereo Pipeline, constitutes a good alternative. Four DTMs, covering the global dichotomy boundary between the southern highlands and northern lowlands along the line of the presumable Arabia shoreline, were produced and analysed. One of them included forms that are likely to be indicative of an oceanic basin that extended across the lowland northern hemisphere of Mars in the geological past. The high resolution DTMs obtained were used in the process of landscape visualisation.

Keywords: Arabia shoreline, Ames Stereo Pipeline, HiRISE, shoreline, landscape visualisation

1. Introduction

Mars appears to be a cold and dry planet. Currently, it is located beyond the Sun's habitable zone, close to its boundary, as defined by Kasting et al. (1993), i.e., beyond the zone in which water in a liquid state may be found on the planet's surface. Additionally, *c.* 4 Ga years ago Mars lost a large part of its atmosphere (Webster et al., 2013), and current low temperatures and atmospheric pressures preclude the presence of flowing or standing water. However, during the last decades of Red Planet exploration evidence has been gathered that such climatic conditions were not a permanent feature.

Second to Earth, Mars is the most intensely investigated planet of our Solar System. To date, over 40 missions have been sent to Mars. Many of them were completed successfully (Brown et al., 2013) and provided a great amount of valuable data. The greatest volume of information on the Red Planet was gathered by two NASA missions: of the Mars Global Surveyor (MGS; NASA, duration: 1997 – 2006) and the Mars Reconnaissance Orbiter (MRO; NASA, duration: 2006 – now). The ESA mission of the Mars Express orbiter (duration: 2003 – now) has also been providing a significant number of valuable data. Mars Orbiter Laser Altimeter (MOLA) and the Mars Orbiter Camera (MOC) are two of five research instruments on board of MGS, several of which have contributed to a detailed exploration of the surface of Mars. MOC included two wide-angle cameras and a narrow-angle one providing images of spatial resolution of up to 1.4 m/pixel (Malin et al., 2010). Height measurements taken by the laser altimeter (MOLA), with a precision of 30 m (or more detailed), were used to produce a global DTM (Digital Terrain Model) of the entire planet at a resolution of 128 pixels/degree. MRO carries on board

two high-resolution cameras: the Context Camera (CTX) and the High Resolution Imaging Science Experiment (HiRISE). CTX acquires images of a spatial resolution of 6 m/pixel across a ~30 km swath (Malin et al., 2007). With the HiRISE camera, images of a submeter (up to ~30 cm/pixel) spatial resolution may be taken across a ~6 km swath (McEwen et al., 2007). Another on-board scientific instrument – CRISM (Compact Reconnaissance Imaging Spectrometer for Mars) provides 18 m/pixel mineralogical data of the surface of Mars (Mustard et al., 2008). Mars Express is equipped with two surface investigation instruments: a High Resolution Stereo Camera (HRSC) and an Observatoire pour la Minéralogie, L'Eau, les Glaces et l'Activité (OMEGA). HRSC acquires colour images across a 52.2 km swath (10 m /pixel spatial resolution) and 2.3 x 2.35 km area at 2.3 m/pixel spatial resolution (Neukum et al., 2004). OMEGA is a spectrometer operating in visible near-infrared wavelength range, capable of mapping the mineral composition of the surface of Mars at 0.3–5 km spatial resolution (Bibring et al., 2005).

Observations from the orbit have enabled identification of land forms such as alluvial fans, deltas and valley networks resembling Earth's river valleys (e.g., Malin & Edgett, 2003; Moore & Howard, 2005; Wood, 2006), layered rock units (e.g., Malin & Edgett, 2000; Grotzinger & Milliken, 2012) that are likely to indicate the presence of water in liquid state on the ancient surface of the planet.

Another indication of the existence of aqueous environments existence on ancient Mars was provided by the Mars Exploration Rover Opportunity. In the Eagle crater located in Meridiani Planum, Opportunity observed and investigated sedimentary rocks rich in hydrated sulphate minerals (Squyres et al., 2004). *In situ* discoveries were confirmed from orbit by OMEGA and CRISM spectrometers. Observations of the mineral composition of the surface of Mars by OMEGA spectrometer have demonstrated the presence of hydrated silicates (pyllosilicates) and sulphates of aqueous origin (Bibring et al., 2005). Pyllosilicates formed during the Noachian period, under alkaline water conditions, possibly at or near the surface which implies the presence of a large water-filled basin (Poulet et al., 2005; Bibring et al., 2006). However, it is possible that the pyllosilicates formed in the deeper subsurface as a result of hydrothermal processes or as a result of impacts and thus would not have needed longstanding water reservoirs (Poulet et al., 2005). Hydrated sulphates, detected by OMEGA, are younger. They formed during the late Noachian to the Hesperian under different, more acidic pH conditions (Bibring et al., 2006). The presence of water during their formation is required, but not necessarily in a longstanding water-filled basin (Bibring et al., 2005). The CRISM spectrometer confirmed previous OMEGA observations of pyllosilicates and provided even more precise data on their mineral diversity and spatial distribution (Mustard et al., 2008). The occurrence of water on Mars was also confirmed by Mars Science Laboratory rover Curiosity in Gale Crater. Already at the beginning of its mission, Curiosity encountered and photographed rocks most likely originating from fluvial transport (Williams et al., 2013; Grotzinger et al., 2014). The finding of water, in the amount of *c.* 2 per cent in the sample of Martian soil examined, was another significant discovery (Leshin et al., 2013). The most important piece of evidence came from Yellowknife Bay, where Curiosity discovered an ancient habitable environment – a palaeo-lake with conditions suited to support life (Grotzinger et al., 2014).

Conditions necessary for the presence of a global hydrological system were best documented for the period between 4.1 and 3.7 Ga, the Noachian, during which many Martian valley networks came into being. The successive period, the Hesperian (3.7–3.0 Ga), including i.e. the development of the majority of the large discharge channels, may have also shown conditions allowing for the presence of episodic water on the planet's surface (Carr & Head, 2010). The above-mentioned dates may be impacted by a large error margin, because the chronology of Mars, calibrated against lunar data and based on numbers of craters, is imperfect in many respects according to our present-day state of knowledge (Hartmann et al., 2001).

It is not clear whether the favourable conditions during the Noachian were stable enough to permit persistent functioning of large water-filled basins on the surface (the "warm and wet Mars" hypothesis). Fairén (2010) suggested that the hypothetical palaeo-ocean resembled the Earth's polar zone oceans (the "cold and wet Mars" hypothesis) and may have even been separated from land by an ice barrier (Fairén et al., 2012).

Regardless of which hypothesis is favoured, Mars's global dichotomy imposes the location of the primordial ocean in the northern hemisphere and its lowland areas discussed here (Parker & Currey, 2001; Carr & Head, 2010), situated on average 5.5 km below the highland areas of the southern hemisphere. Apart from differences in elevation, the term 'global dichotomy' refers to crust thickness and surface age (measured by crater density) differences between the northern and southern hemispheres (Nimmo & Tanaka, 2005). The northern

ocean likely covered even up to 30 per cent of the planet's surface (Clifford & Parker, 2001). However, considering the assumed age of the ocean (early Noachian/late Hesperian), a great part of its geomorphological record may have been obliterated at present (Head et al., 2002).

Clifford & Parker (2001) identified and suggested a number of global and local contacts on the basis of low-resolution Viking orbiter imagery and earlier data from the Mars Global Surveyor mission, including MOC imagery and MOLA DTM. With a gradual increase in the wealth and quality of MGS data, these were verified, e.g. by Carr & Head (2003) and Webb (2004), but also criticised, e.g. by Ghatan & Zimbelman (2006). Various landforms such as scarps, ridges and terraces were discussed as possible traces of wave-erosion of the palaeo-ocean. In many cases detailed examination of a high-resolution satellite imagery supported by the most accurate DTM data available at the time (MOLA, ~300 m along-track spacing between measurements and vertical accuracy of a minimum of 30 m) called such interpretation into question, and other scenarios of origin were proposed (Barnhart et al., 2005; Ghatan & Zimbelman, 2006). Only few candidates have withstood such evaluation; however, it remains clear that the resolution of MOLA DTM could be insufficient to understand their morphology fully. Especially in context of Martian wave energy models presented by Kraal et al. (2006) that revealed that even with favourable input conditions, shoreline features could reach only up to ~5 m in height. Such forms require DTM of much higher spatial resolution and vertical accuracy than MOLA.

In order to identify and visualise possible traces of erosive activity in the palaeo-ocean, four potentially interesting areas, including one previously examined by Clifford & Parker (2001) and evaluated by Ghatan & Zimbelman (2006), were selected along one of the hypothetical global shorelines, the Arabia contact (Fig. 1) proposed by Webb (2004). For each of them, a Digital Terrain Model (DTM) was produced from stereoscopic High Resolution Imaging Science Experiment (HiRISE) imagery. This paper presents a geomorphological analysis of HiRISE DTMs located at the dichotomy boundary near the edge of Arabia Terra along the line of the Arabia contact (Fig. 1).

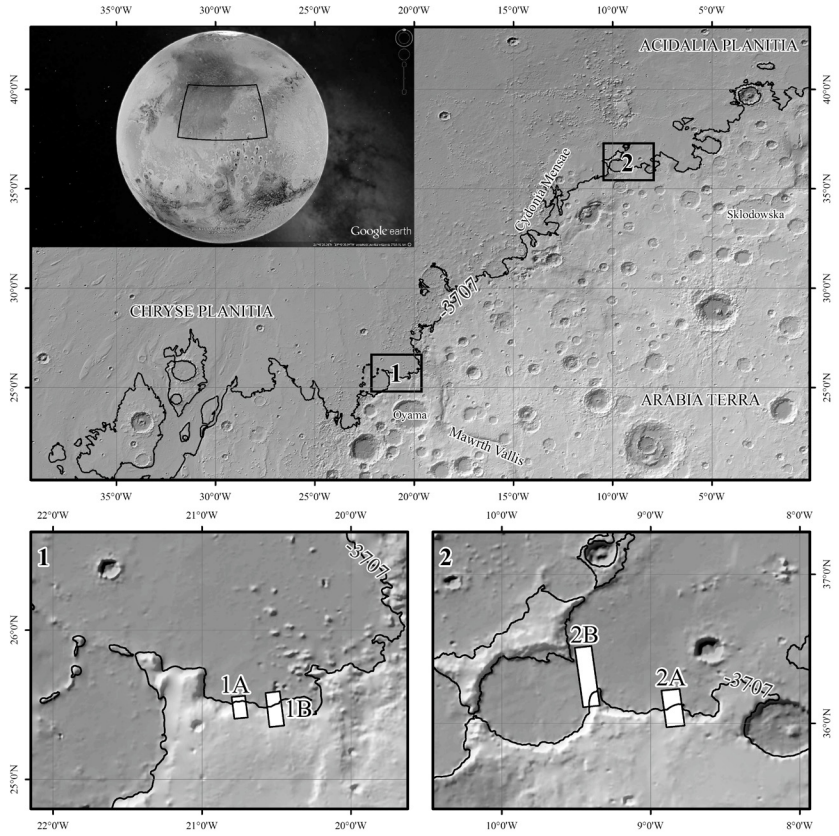

Fig. 1. Localisation of the study areas on MOLA DTM shaded relief. Black lines represent elevation –3707 m (Arabia contact according to Webb, 2004). White polygons marked 1A, 1B, 2A and 2B indicate the common extent of each stereo pair. Mars simple cylindrical projection. Google Earth image of Mars globe provided by NASA/USGS and ESA/DLR/FU Berlin

2. Methods

The study areas were selected on the basis of available HiRISE stereo pairs showing the line of the Arabia contact. The height of this contact was estimated at –3707 m by Webb (2004), in a DTM generated from point MOLA measurements.

Two areas were chosen for analysis. The first one is situated in the region of Mawrth Vallis (Fig. 1). According to MOLA data, this area includes a rim of a highland, separating relatively poorly diversified lowland of the Chryse Planitia from the *c.* 800 m higher Arabia Terra to the southeast. The line of the Arabia contact runs along the rim. DTMs presenting a fragment of area extending along the Arabia contact were generated from two HiRISE stereo pairs:

- ESP_030200_2060 and ESP_030622_2060 (1A),
- ESP_027378_2060 and ESP_027655_2060 (1B).

The second of the areas analysed (Fig. 1) is situated ~900 km to the northeast, on the boundary of Arabia Terra, near Cydonia Mensae. MOLA data indicate several large craters with partly eroded rims located along the boundary of the highland. High-resolution DTMs illustrating the area along the Arabia contact were produced from the following HiRISE stereo pairs:

- PSP_001414_2165 and PSP_001968_2165 (2A),
- ESP_025360_2165 and ESP_025650_2165 (2B).

All data used in the present study (MOLA, HiRISE) were downloaded from archives of the Planetary Data System (McMahon, 1996; Hare, 2010). DTMs were developed with the ISIS3 (USGS, http://isis.astrogeology.usgs.gov), Ames Stereo Pipeline (NASA, http://ti.arc.nasa.gov/tech/asr/intelligent-robotics/ngt/stereo/) and ArcGIS (ESRI) software. ISIS3 (Integrated System for Imagers and Spectrometers) enables processing of remote sensing data and is particularly oriented towards data obtained during the NASA missions (Gaddis et al, 1997).

Ames Stereo Pipeline (ASP) is a set of tools for automated processing of stereophotogrammetric remote sensing data collected from the orbit or planet surface. It supports, amongst others, development of DTMs from stereoscopic satellite imagery (Broxton & Edwards, 2008; Moratto et al., 2010). DTMs were produced from EDR (Experiment Data Record) data collected by each of HiRISE 10 red light (550–850 nm) detectors, using the procedure introduced by NASA Ames Research Center (2013) (Fig. 2, Steps 1–5). DTM generated in the ASP was verified and appeared to vary from the MOLA PEDR point data (PEDR – Precision Experiment Data Record). In order to minimise this variance,

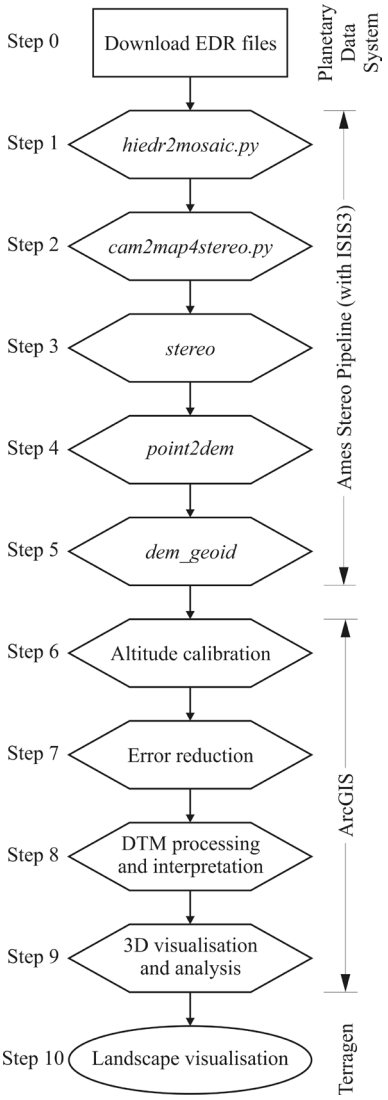

Fig. 2. DTM production process. ASP scripts and programs are italicised (NASA Ames Research Center, 2013). Step 1: Mosaic and calibration of particular HiRISE red light detector images. Step 2: Alignment of mosaic left and right images of stereo pair and determining their common extent. Step 3: Generating point cloud data from overlapping stereo pair images. Step 4: Producing DTM in a GeoTIFF format from the point cloud data with left image orthorectification. Step 5: Matching HiRISE DTM reference system with MOLA areoid (Smith et al., 2001) to compare resultant data with previous research. Step 6: Identifying and minimising height differences between computed DTM and reference MOLA PEDR point measurements. Step 7: Identification and correction of DTM errors. Step 8: Applying methods (hill-shading, Topographic Position Index) to enhance DTM interpretation potential. Step 9: 3D visualisation of DTM surface and other (optical, TPI) data draped on DTM. Step 10: Rendering visualisations of present-day and ancient Martian landscapes

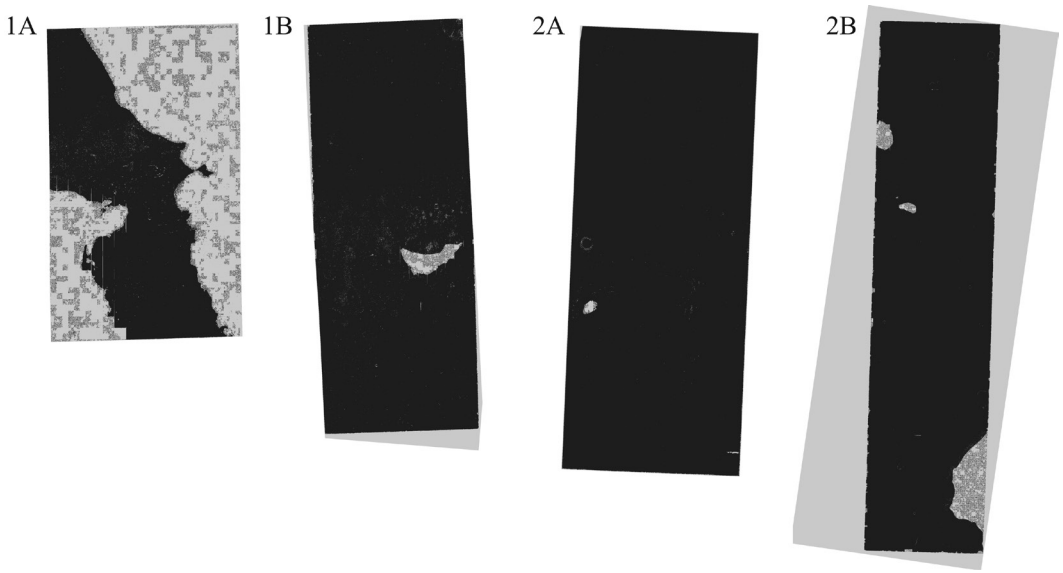

Fig. 3. 'Good-pixel map' images for each stereo pair produced by Ames Stereo Pipeline. 1A, 1B, 2A and 2B represent particular stereo pairs. The light grey colour indicates areas of misaligned pixels. Continuous dark grey areas represent data of good quality

PEDR measurements from the stereo pair overlap were used to calculate the mean height difference between the DTM and MOLA PEDR (Table 1). This value was used to calibrate the resultant data (Fig. 2, Step 6).

In bland areas, either feature less or with very steep slopes, some artefacts (no-data pixels) could be introduced to the model (Kirk et al., 2008). The distribution of such artefacts is shown on the so-called "good pixel map" (Fig. 3), produced by ASP. Small (≤ 10 pixels) discontinuous areas were filled with mean values of the surrounding pixels (*FocalStatistic* command, ArcGIS). Some larger voids in the DTMs were filled in manual contour line interpolation (Fig. 2, Step 7). Other possible errors, presented in Fig. 4, result from the specificity of the HiRISE instrument and algorithms applied by the software for calibration (Kirk et al., 2008). It should be emphasised that the processing steps described yield good quality data for geomorphological

Table 1. Height differences between computed DTMs and MOLA PEDR measurements

	Stereo pair			
	1A	1B	2A	2B
Number of MOLA PEDR points	53	119	119	392
Minimum height difference (m)	125.99	105.64	80.02	153.57
Maximum height difference (m)	176.12	147.42	128.48	239.63
Mean height difference (m)	**153.83**	**134.14**	**110.72**	**190.32**
Standard deviation (m)	13.09	6.72	8.06	7.64

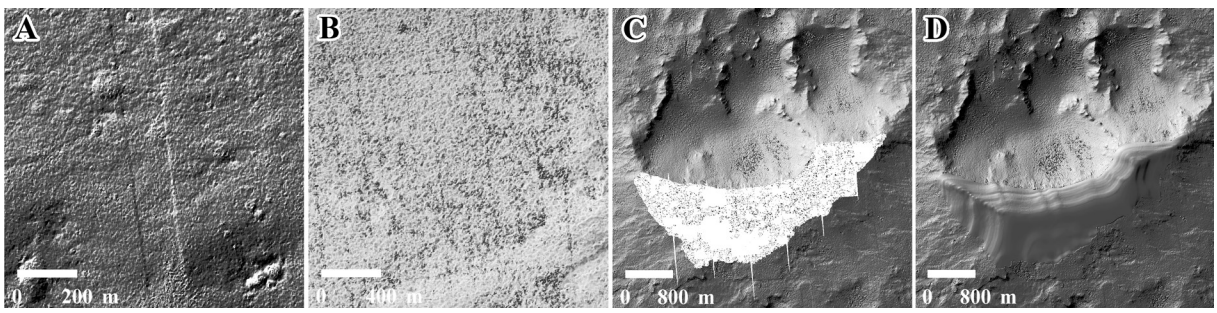

Fig. 4. Examples of errors afflicting the DTM production process
A – Seams result from small differences in images taken by particular HiRISE CCDs (Kirk et al., 2008); **B** – Barely visible "check" pattern coming out of algorithms used in ASP software; **C** – No-data areas that occur in zones of very low contrast or very stepped slopes; **D** – Result of their manual interpolation

analysis. However, for data of critical importance (e.g. for selection of landing sites) a higher quality should be ensured in a human-based photogrammetric process, to be carried out by an experienced operator (compare with Kirk et al., 2008).

To visualise and interpret the data, morphological profiles and derivatives of the DTM, i.e., the hillshade model and the Topographic Position Index, were generated (Fig. 2, Step 8). The hillshade model was created by illuminating DTM by a light source. It is a widely used method to visualise terrain data (Kennelly, 2008).

Topographic Position Index (TPI) belongs to a large set of morphometric parameters and is a calculation of the relative position of each DTM pixel in relation to the mean height of the surrounding pixels (Tagil & Jenness, 2008; de Reu et al., 2013). TPI greatly enhances even small convexities and concavities of surfaces which allow to recognise even marginal morphological forms. The data were 3D visualised and interpreted with the help of ArcGIS ArcScene (ESRI) (Fig. 2, Step 9).

Terragen (Planetside Software) (Fig. 2, Step 10) software was used to produce photorealistic landscape visualisations. Images were generated on the basis of a network of shaders, determining the appearance of particular landscape components. Software functions allow for a detailed control of the terrain model, coverage of ground surface, lighting and atmosphere. Imported geodata, previously processed with GIS software, may provide a basis for realistic landscape reconstructions, both in static images and animations.

3. Results and discussion

DTMs processed for particular stereo pairs are presented in Fig. 5. For stereo pair ESP_030200_2060 / ESP_030622_2060 (1A), automatic correlation resulted in low-quality data. The generated DTM attained a pixel size of ~0.48 m. However, it included numerous unmatched raster cells, which is why stereo pair 1A was excluded from further analyses.

DTM prepared for the ESP_027378_2060 / ESP_027655_2060 (1B) stereo pair, with a pixel size of ~0.47 m was of high quality. Only the eastern part of the area included a no-data site that required manual interpolation. The boundary separating the highland Arabia Terra from the lower-lying Chryse Planitia is easily recognised in the model (Fig. 6) and extends in a smooth zone between –3700 and –3600 m. The DTM HiRISE contour line of –3707 m runs in the central part of the area. Its outline varies from the DTM MOLA contour line of –3707 m, as the grid MOLA DTM was interpolated from point data (spatial resolution: 128 pixels/degree) distributed along particular MGS orbits.

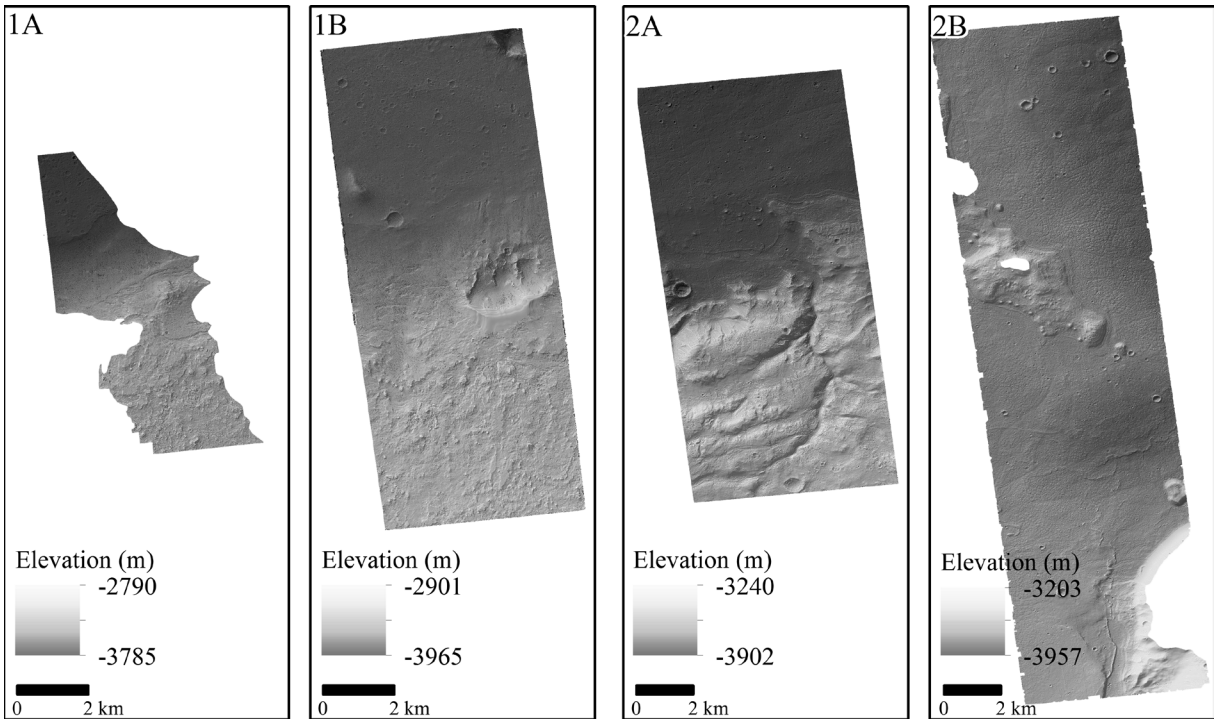

Fig. 5. Results of the DTM production process. Location of particular DTMs corresponds to common extents of each stereo pair as marked in Fig. 1

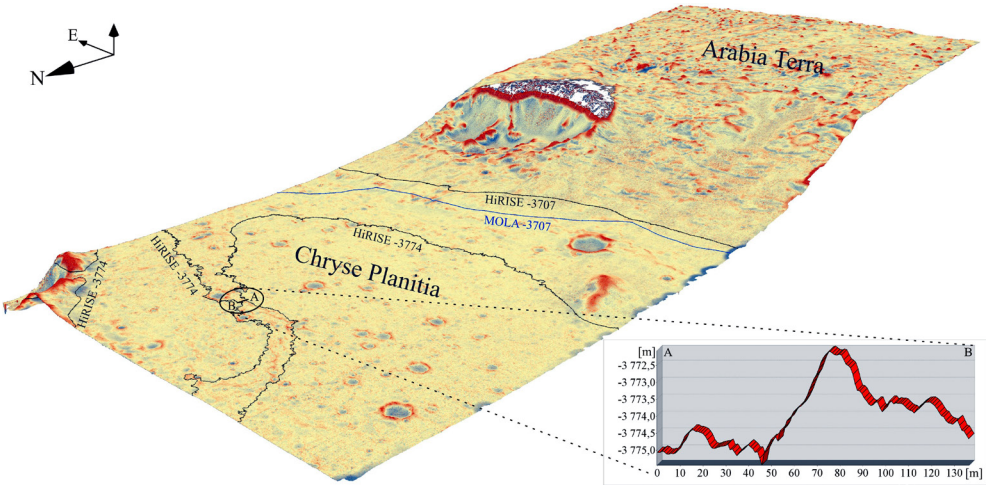

Fig. 6. Perspective view of area 1B composed of draped TPI on HiRISE DTM. Vertical exaggeration x2. Red areas are convex, blue areas concave with regard to their surroundings. Dark grey contours represent elevation from HiRISE DTM, the blue one represents elevation from MOLA DTM

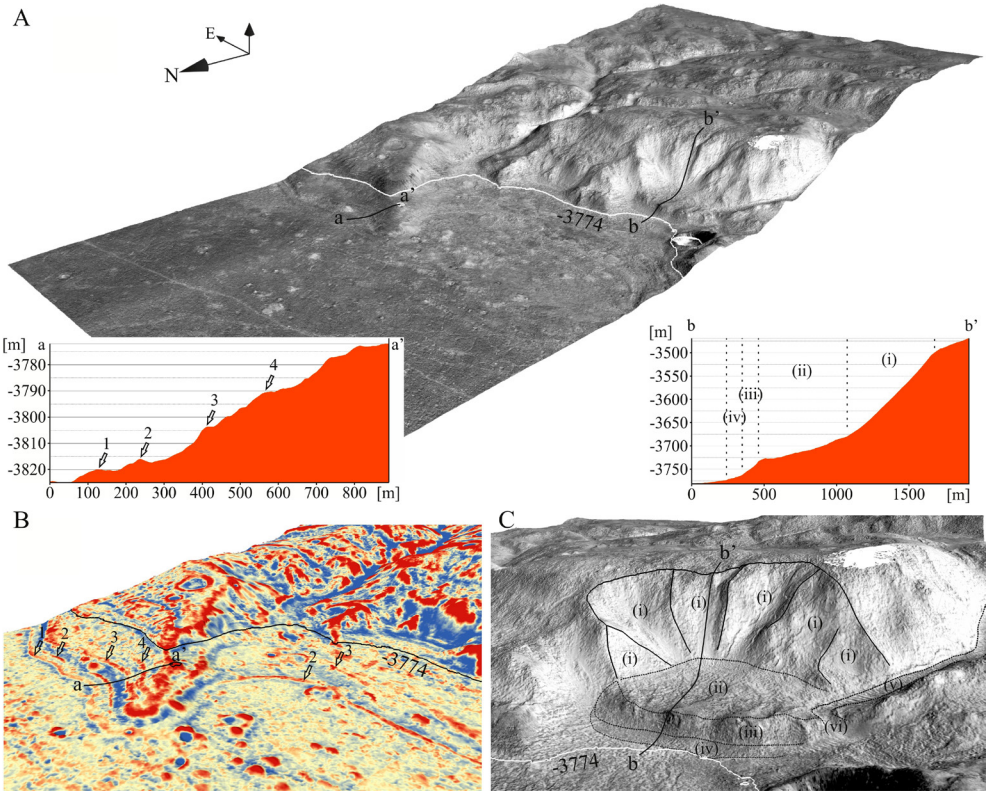

Fig. 7. Perspective views of area 2A. Vertical exaggeration x3.
A – Composition of draped HiRISE optical data on HiRISE DTM with localisation of –3774 contour and profiles aa' and bb'; **B** – Composition of draped TPI on HiRISE DTM. Red areas are convex, blue areas concave with regard to their surroundings. Strandlines are marked by arrows and numbered on both perspective view and profile aa'; **C** – Composition of draped HiRISE optical data on HiRISE DTM. The observed complex gully form consists of six alcoves, marked (i), collective fan, (ii) terminated at steep scarp (iii). Area marked (iv) shows extent of darker fan material at foot of scarp. To the right is a channel (v) with its apron (vi) blocked by the fan material

Relief, enhanced by the TPI (Fig. 6), does not show erosional signatures of a palaeo-ocean nearby the Arabia shoreline (–3707 m) proposed by Webb (2004). In the central part, a large landslide (width: ~2.5 km, surface area: ~3 km^2, vertical range: ~300 m) may be observed. Figure 6 includes contour lines of –3774 m (described below on stereo pairs 2A and 2B), in the northern part of the area adjacent

to a small ridge (length: ~3.5 km, height: ~2 to ~4 m, width: *c*. 30 m). Data available are insufficient to determine the origin of the ridge. The northeastern corner of the area comprises a fragment of a crater with partly eroded rim forming a "gate". The basal part of the rim is located at a height of –3775 m, while the depression at the gate's floor is at –3785 m. No traces of processes that led to its formation were found.

In the area presented in stereo pair PSP_001414_2165/PSP_001968_2165 (2A), the boundary of topographic dichotomy separating the lowland in the north from the southern highland extends in a zone attaining a height of *c*. –3760 m (Fig. 7). This boundary overlaps a rim of a crater, about 60 km in diameter, and is marked by numerous parallel rims referred to as "strandlines" (Clifford & Parker, 2001) that may be observed across the entire area. Ghatan & Zimbelman (2006) considered that such an interpretation was possible, yet also indicated other feasible developmental scenarios, such as ground ice flow or wind action. The produced DTM allowed retrieval detailed position and size of putative strandlines. At heights between –3823 m and –3750 m, these are recorded at intervals of a several dozen metres and are 0.5–4 m in height and ~20 m in width (Fig. 7B). These parameters may be compared with palaeo-shoreline traces described by Ghatan & Zimbelman (2006) from the Long Valley, Nevada.

The western part of the highland boundary includes a complex poleward facing form developed by gravity-driven downslope processes (width: ~1.7 km, surface area: ~2 km^2, vertical range: ~300 m) (Fig. 7C). It is similar to some types of relatively young (Amazonian age) morphological forms, known as gullies (Dickson & Head, 2009; Auld & Dixon, 2014). However, its indistinct morphology suggests an older age. The gully described probably developed prior to or simultaneously with the valley located to the west to it, because the valley is blocked by gully fan and the valley's outlet is carved within the fan material. The entire form is composed of six alcoves with collective fan. The fan itself is abruptly terminated near the –3774 m contour line, and its apron forms a steep ramp, > 40 m in height. Such fan morphology possibly is the result of wave-cut erosion and contrasts with younger, poleward facing gullies observed at the same latitudes (Dickson & Head, 2009) where fan material overflows without restraint and often forms lobate debris aprons. The gully also lacks distinctly V-shaped channels which suggest mass wasting processes (Auld & Dixon, 2014) as its main forming factor. The area to the northeast of the gully comprises a meteorite crater of a clear, fresh relief, most likely formed after recession of the palaeo-ocean. The southern, strongly diversified part of the area is covered by a valley network with its outlet located at the dichotomy boundary.

Figure 8 presents a photorealistic visualisation of Martian landscape and reconstruction of its possible appearance during the Noachian. DTM produced from stereo pair 2A served as input data. The appearance of ground surface, including loose rock fragments, colour and transparency of atmosphere and lighting were reconstructed on the basis of photographs taken on the surface of Mars by Spirit, Opportunity and Curiosity rovers. In the reconstruction, the appearance of atmosphere and lighting was deduced from Curiosity photographs. However, their white balance was modified towards a colour scheme typical of the Earth.

The area covered by stereo pair ESP_025360_2165/ESP_025650_2165 (2B) is located *c*. 35 km to the northwest of area 2A. The DTM produced (pixel size: ~0.52 m) was mostly of high quality, but did include three large no-data areas. The model covers a junction of two sediment-filled craters (Fig. 9): a smaller, younger one (I), *c*. 45 km in diameter found in the southwestern part of the area, and a larger one (II), 60 km in diameter and observed in the northeast.

The floors of both craters are covered largely by contraction-crack polygons of a relief more easily recognised in crater (II), of lower locations. On Earth, similar structures are to be found in periglacial environments (Marchand & Head, 2007) such as the Antarctic Dry Valley. The basal part of crater (I) is marked by numerous, mostly sinuous shaped ridges (Fig. 9 C), elevated ~2 to 8 m above their surroundings. Ridges are about 30 to 150 m wide and continue in two general directions: west-east and south-north. Their occurrence is not likely to be linked to relief-forming activity in the ocean. Possibly, they originate from a later period having formed during the movement and subsequent disappearance of ice cover. The presence of such structures suggests a phase of climatic cooling resulting in freezing of the ocean.

The rim of the crater (I), separating it from the deeper crater (II), extends in a northwest-southeast direction in the central part of the area and attains an elevation of –3860 m and above. The entire rim is marked by numerous ramparts. The most notable ones are elevated ~2 m above their surroundings. The highest part of the ridge, above –3774 m, is nearly completely inapparent due to incorrect matching of pixels in stereo pair 2B. In its correct fragment in the DTM, the slope shows a greater inclination

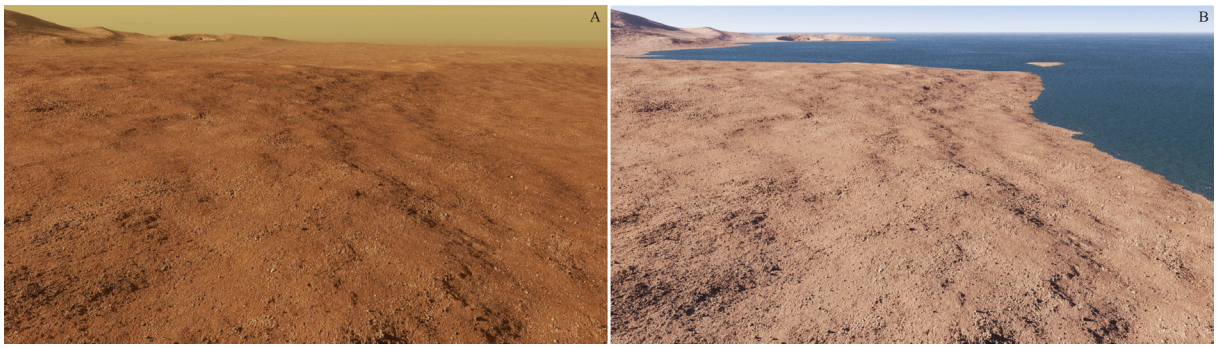

Fig. 8. Visualisations of the landscape of Mars. Views, from the east, on the possible Arabia shoreline (**A**) as seen today, (**B**) what it might have looked like during the Noachian period

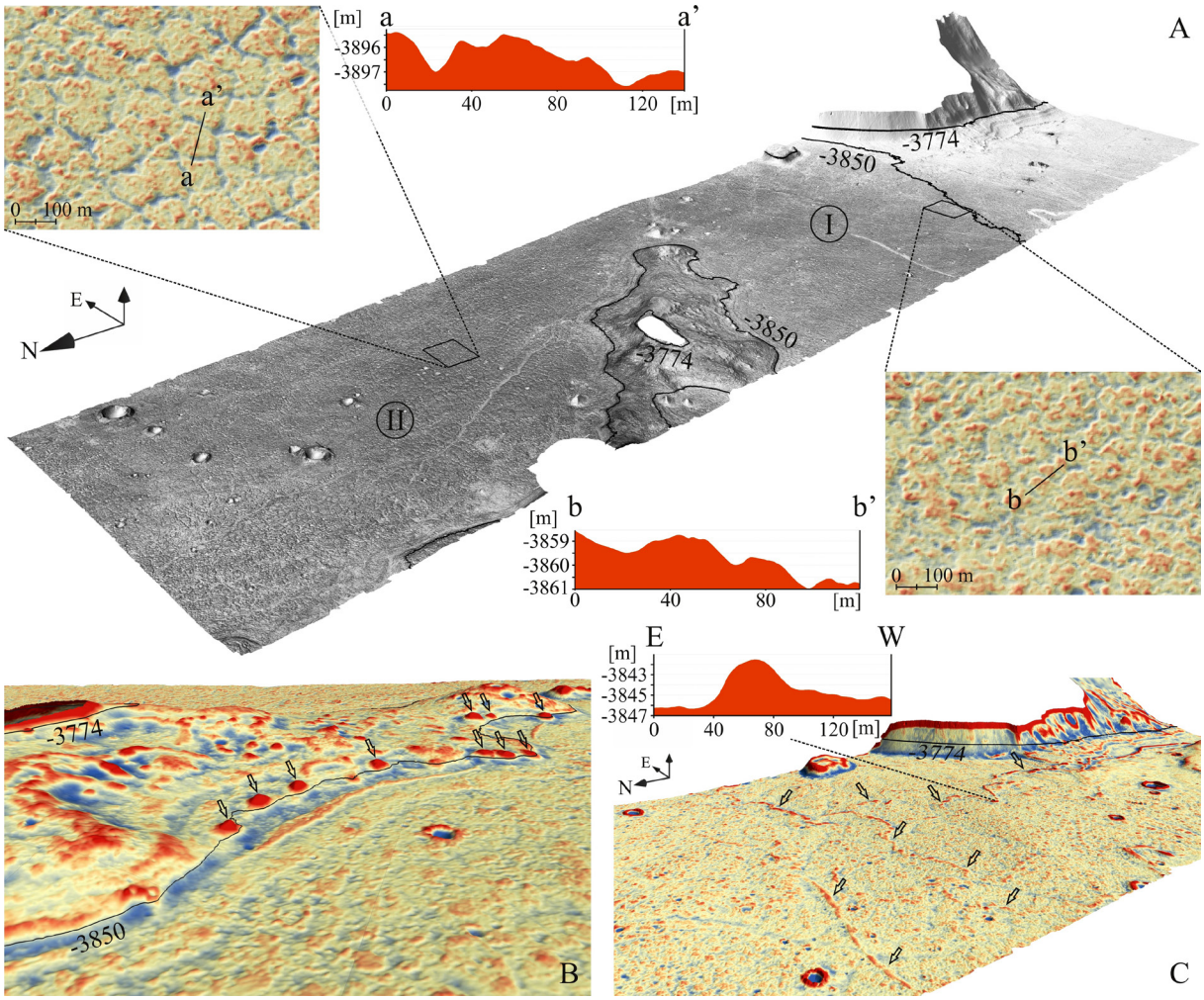

Fig. 9. Perspective views of 2B. Vertical exaggeration x3

A – Composition of draped HiRISE optical data on HiRISE DTM with localisation of –3774 and –3850 contours. Numbers (I) and (II) indicate the two craters mentioned in the text. Close-look images (TPI, red areas are convex, blue ones concave with regard to their surroundings) and associated profiles show typical contraction-crack polygons at crater floors (I) and (II); **B, C** – Images are compositions of draped TPI on HiRISE DTM. Red areas are convex, blue ones concave with regard to their surroundings; **B** – Close-look from the southwest on the rim between craters. Arrows point to hummocky landforms mentioned in the text; **C** – View from the northwest on the southern part of area. Arrows and associated profile point to narrow ridges interpreted as remnants of glaciation within Acidalia Planitia

angle at the peak than in the southeastern extension of the form. Therefore, either the peak was formed of rocks of greater resistance or erosion activity was stronger at lower heights. If the long-lasting level of palaeo-ocean was estimated at –3774 m, as concluded from DTM of area 2A, the peak of crater rim would be a small island. The peak observed on a source ESP_025360_2165 image appears to be a featureless area, with clearly distinguishable texture compared to the rim's northern steep slope. A similar texture change, marked by a sharp edge, is seen on the southern slope at heights between –3780 m (western part) and –3806 m (eastern part). This level is also the location of the upper edge of the landslide of the southern side of the crater rim. The edge continues at a height of *c*. –3815 m, in an isolated fragment of crater rim situated further to the southeast.

Figure 9 includes ten isometric, dome-shaped, discrete hummocky landforms found at the same height (*c*. –3850 m), along the bottom part of the crater rim. The forms attain *c*. 90–180 m in diameter and are elevated *c*. 10–14 m above the surrounding surface. On the slope, their linear distribution clearly indicates a trimline that may be associated with the gradual disappearance of ice cover from the crater. A fragment of the crater (I) rim, visible in the southeastern corner of the area, forms the boundary of the Arabia Terra plateau. The peak of the rim is inapparent due to errors in DTM generation. However, this rim is much higher and steeper than the one separating craters (I) and (II). Its slope inclination noticeably increases above –3774 m, suggesting the presence of a cliff coast in the region.

4. Conclusions

MOLA DTM provides an excellent image of Mars landforms at both regional and planetary scales. However, the resolution is insufficient to identify relief details at a larger scale. Such analyses require data of higher spatial resolution. At present, the most detailed images of the surface of Mars are provided by the HiRISE. The extensive library of available HiRISE imagery enables identification and analysis of relief details from the surface of Mars with submeter precision. In stereoscopic coverage, these data may provide a basis for very detailed DTM. Currently, the Planetary Data System catalogue includes over 3,500 stereo pairs. However, only *c*.160 DTMs based upon them are available in practice, because manual processing of each pair is time-consuming. Automated analysis using the Ames Stereo Pipeline and ISIS3 software serves as a great alternative for human-based photogrammetric process. An undoubted advantage of ASP and ISIS3 software is their distribution under free software license. Both the human-based photogrammetric process and automated processing of stereoscopic HiRISE imagery may be affected by errors. However, models developed automatically often are of high quality.

Production of DTMs from HiRISE stereo pairs significantly increases their interpretation potential, by providing the opportunity to use morphometric parameters, enabling the observation of fine relief details that were indistinct in the original images. Detailed DTMs may be used to generate photorealistic visualisations, helpful in spatial data analyses and providing an attractive form of landscape presentation.

Two of four DTMs analysed, covering an area located near Mawrth Vallis (Fig. 1. locations 1A and 1B), did not include clear traces of presence of a water-filled basin. In consideration of age and geological setting of the region interpreted, such traces may have been partially destroyed or masked by subsequent processes.

However, analysis of the 2A DTM, of the area near Cydonia Mensae (Fig. 1. location 2A), has resulted in identification and description of forms associated with relief-forming activity in the Martian palaeo-ocean. The forms distinguished include numerous rims, possibly remains of a palaeo-shoreline and a steep fan apron developed possibly as a result of wave-cut erosion. In the study area, they extend to the level of –3774 m which could indicate the long-standing extent of the Martian palaeo-ocean during the Noachian.

DTM developed from stereo pair 2B comprised morphological traces of a phase of climatic cooling in the geological history of Mars, resulting in freezing of the gradually receding ocean, although there is no direct evidence for shorelines at the previously assumed level. Therefore, at many sites the outline of the palaeo-shoreline may have been remodelled by later glacial processes.

Acknowledgements:

The author wishes to thank the HiRISE and MOLA teams for collecting the data and ISIS3 and ASP teams for creating and sharing their software, and Jerzy Zasadni and Marek Wendorff for their comments. Helpful comments by Tom van Loon and an anonymous reviewer are much appreciated. This research study was supported by AGH University of Science and Technology grant 11.11.140.175.

References

Auld, K.S. & Dixon, J.C., 2014. Classification of Martian gullies from HiRISE imagery. *Lunar and Planetary Institute Science Conference Abstracts* 45, 45th Lunar and Planetary Science Conference, Woodlands, USA. LPI Contribution 1777, 1270.

Barnhart, C.J., Tulaczyk, S., Asphaug, E., Kraal, E.R. & Moore, J., 2005. Ice-ridge pile up and the genesis of Martian "shorelines". *Lunar and Planetary Institute Science Conference Abstracts* 36, 36th Lunar and Planetary Science Conference, League City, USA. LPI Contribution 1560.

Bibring, J.-P., Langevin, Y., Gendrin, A., Gondet, B., Poulet, F., Berthé, M., Soufflot, A., Arvidson, R., Mangold, N., Mustard, J., Drossart, P. & the OMEGA team, 2005. Mars Surface Diversity as Revealed by the OMEGA/Mars Express Observations. *Science* 307, 1576-1581, doi: 10.1126/science.1108806.

Bibring, J.-P., Langevin, Y., Mustard, J.F., Poulet, F., Arvidson, R., Gendrin, A., Gondet, B., Mangold, N., Pinet, P., Forget, F. & the OMEGA team, 2006. Global Mineralogical and Aqueous Mars History Derived from OMEGA/Mars Express Data. *Science* 312, 400–404, doi: 10.1126/science.1122659.

Brown, D., Cole, S., Webster, G., Agle, D.C., Chicoine, R.A., Rickman, J., Hoover, R., Mitrofanov, I., Ravine, M., Hassler, D., Cuesta, L., Jones, N.N., Barnstorff, K., Faccio, R., Apuzzo, M.L.J. & Pagán, V.M., 2013. The Mars Science Laboratory Landing. *World Neurosurgery* 79, 223–242.

Broxton, M. & Edwards, L., 2008. The Ames Stereo Pipeline: Automated 3D surface reconstruction from orbital imagery. *Lunar and Planetary Institute Science Conference Abstracts*, 39, 39th Lunar and Planetary Science Conference, League City, USA. LPI Contribution 1391, 2419.

Carr, M.H. & Head, J.W., 2003. Oceans on Mars: An assessment of the observational evidence and possible fate. *Journal of Geophysical Research*, 108, E5, 5042, 1–28, doi: 10.1029/2002JE001963.

Carr, M.H. & Head, J.W., 2010. Geologic history of Mars. *Earth and Planetary Science Letters* 294, 185–203.

Clifford, S.M. & Parker, T.J., 2001. The evolution of the Martian hydrosphere: Implications for the fate of a primordial ocean and the current state of the Northern plains. *Icarus* 154, 40–79.

De Reu, J., Bourgeois, J., Bats, M., Zwertvaegher, A., Gelorini, V., De Smedt, P., Chu, W., Antrop, M., De Maeyer, P., Finke, P., Van Meirvenne, M., Verniers, J. & Crombé, P., 2013. Application of the topographic position index to heterogeneous landscapes. *Geomorphology* 186, 39–49.

Dickson, J.L. & Head, J.W., 2009. The formation and evolution of youthful gullies on Mars: Gullies as the late-stage phase of Mars' most recent ice age. *Icarus* 204, 63–86, doi:10.1016/j.icarus.2009.06.018.

Fairén, A.G., 2010. A cold and wet Mars. *Icarus* 208, 165–175.

Fairén, A.G., Davila, A.F., Schulze-Makuch, D., Rodríguez, J.A.P. & McKay, C.P., 2012. Glacial paleoenvironments on Mars revealed by the paucity of hydrated silicates in the Noachian crust of the Northern Lowlands. *Planetary and Space Science* 70, 126–133.

Gaddis, L.,Anderson, J., Becker, K., Becker, T., Cook, D., Edwards, K., Eliason, E., Hare, T., Kieffer, H., Lee, E. M., Mathews, J., Soderblom, L., Sucharski, T., Torson, J., McEwen, A. & Robinson, M., 1997. An Overview of the Integrated Software for Imaging Spectrometers (ISIS). *Proceedings of the 28th Annual Lunar and Planetary Science Conference*, Houston, USA, Abstract 1226. 387–388.

Ghatan, G.J. & Zimbelman, J.R., 2006. Paucity of candidate coastal constructional landforms along proposed shorelines on Mars: Implications for a northern lowlands-filling ocean. *Icarus* 185, doi: 10.1016/j.icarus.2006.06.007.

Grotzinger, J.P. & Milliken, R.E., 2012. The sedimentary rock record of Mars: Distribution, origins, and global stratigraphy, in Sedimentary Geology of Mars. *SEPM Special Publication* 102, 1–48.

Grotzinger, J.P., Sumner, D.Y., Kah, L.C., Stack, K., Gupta, S., Edgar, L., Rubin, D., Lewis, K., Schieber, J., Mangold, N., Milliken, R., Conrad, P.G., DesMarais, D., Farmer, J., Siebach, K., Calef III, F., Hurowitz, J., McLennan, S.M., Ming, D., Vaniman, D., Crisp, J., Vasavada, A., Edgett, K.S., Malin, M., Blake, D., Gellert, R., Mahaffy, P., Wiens, R.C., Maurice, S., Grant, J.A., Wilson, S., Anderson, R.C., Beegle, L., Arvidson, R., Hallet, B., Sletten, R.S., Rice, M., Bell III, J., Griffes, J., Ehlmann, B., Anderson, R.B., Bristow, T.F., Dietrich, W.E., Dromart, G., Eigenbrode, J., Fraeman, A., Hardgrove, C., Herkenhoff, K., Jandura, L., Kocurek, G., Lee, S., Leshin, L.A., Leveille, R., Limonadi, D., Maki, J., McCloskey, S., Meyer, M., Minitti, M., Newsom, H., Oehler, D., Okon, A., Palucis, M., Parker, T., Rowland, S., Schmidt, M., Squyres, S., Steele, A., Stolper, E., Summons, R., Treiman, A., Williams, R., Yingst, A. & MSL Science Team, 2014. A habitable fluvio-lacustrine environment at Yellowknife Bay, Gale Crater, Mars. *Science* 343, 6169, doi:10.1126/science.1242777.

Hare, T.M., 2010. A Case for a PDS Supported Cartographic Raster Library. *Lunar and Planetary Institute Science Conference Abstracts*, 41, 41th Lunar and Planetary Science Conference, Woodlands, USA. LPI Contribution 1533, 2728.

Hartmann, W.K., Kallenbach, R., Geiss, J. & Turner, G., 2001. Summary: New views and new directions in Mars research. *Space Science Reviews* 96, 461–470.

Head, J.W., Kreslavsky, M.A. & Pratt, S., 2002. Northern lowlands of Mars: Evidence for widespread volcanic flooding and tectonic deformation in the Hesperian Period. *Journal of Geophysical Research* 107, 5003; doi: 10.1029/2000JE001445.

Kasting, J.F., Whitmire, D.P. & Reynolds, R.T., 1993. Habitable zones around Main Sequence Stars. *Icarus* 101, 108–128.

Kennelly, P.J., 2008. Terrain maps displaying hill-shading with curvature. *Geomorphology* 102, 567–577, doi: 10.1016/j.geomorph.2008.05.046.

Kirk, R.L., Howington-Kraus, E., Rosiek, M.R., Anderson, J.A., Archinal, B.A., Becker, K.J., Cook, D.A.,

Galuszka, D.M., Geissler, P.E., Hare, T.M., Holmberg, I.M., Keszthelyi, L.P., Redding, B.L., Delamere, W.A., Gallagher, D., Chapel, J.D., Eliason, E.M., King, R. & McEwen, A.S., 2008. Ultrahigh resolution topographic mapping of Mars with MRO HiRISE stereo images: Meter-scale slopes of candidate Phoenix landing sites. *Journal of Geophysical Research* 113, E00A24, 1–31, doi:10.1029/2007JE003000.

Kraal, E.R., Asphaug, E., Moore, J.M. & Lorenz, R.D., 2006. Quantitative geomorphic modeling of Martian bedrock shorelines. *Journal of Geophysical Research* 111, E03001, 1–13, doi:10.1029/2005JE002567.

Leshin, L.A., Mahaffy, P.R., Webster, C.R., Cabane, M., Coll, P., Conrad, P.G., Archer, P.D., Atreya, S.K., Brunner, A.E., Buch, A., Eigenbrode, J.L., Flesch, G.J., Franz, H.B., Freissinet, C., Glavin, D.P., McAdam, A.C., Miller, K.E., Ming, D.W., Morris, R.V., Navarro-González, R., Niles, P.B., Owen, T., Pepin, R.O., Squyres, S., Steele, A., Stern, J.C., Summons, R.E., Sumner, D.Y., Sutter, B., Szopa, C., Teinturier, S., Trainer, M.G., Wray, J.J., Grotzinger, J.P. & MSL Science Team, 2013. Volatile, isotope, and organic analysis of Martian fines with the Mars Curiosity Rover. *Science* 341, 6153, 1–9, doi:10.1126/science.1238937.

Malin, M.C., Bell Iii, J.F., Cantor, B.A., Caplinger, M.A., Calvin, W.M., Clancy, R.T., Edgett, K.S., Edwards, L., Haberle, R.M. & James, P.B., 2007. Context camera investigation on board the Mars Reconnaissance Orbiter. *Journal of Geophysical Research* 112, E05S04, 1–25, doi:10.1029/2006JE002808.

Malin, M. C. & Edgett, K. S., 2000. Sedimentary rocks of Early Mars, *Science* 290(5498), 1927–1937, doi: 10.1126/science.290.5498.1927.

Malin, M. C. & Edgett, K. S., 2003. Evidence for persistent flow and aqueous sedimentation on Early Mars, *Science* 302(5652), 1931–1934, doi: 10.1126/science.1090544.

Malin, M.C., Edgett, K.S., Cantor, B.A., Caplinger, M.A., Danielson, G.E., Jensen, E.H., Ravine, M.A., Sandoval, J.L. & Supulver, K.D., 2010. An overview of the 1985–2006 Mars Orbiter Camera science investigation. *Mars* 5, 1–60.

Marchant, D.R. & Head, J.W., 2007. Antarctic dry valleys: Microclimate zonation, variable geomorphic processes, and implications for assessing climate change on Mars. *Icarus* 192, 187–222, doi:10.1016/j.icarus.2007.06.018.

McEwen, A.S., Eliason, E.M., Bergstrom, J.W., Bridges, N.T., Hansen, C.J., Delamere, W.A., Grant, J.A., Gulick, V.C., Herkenhoff, K.E., Keszthelyi, L., Kirk, R.L., Mellon, M.T., Squyres, S.W., Thomas, N. & Weitz, C.M., 2007. Mars Reconnaissance Orbiter's High Resolution Imaging Science Experiment (HiRISE). *Journal of Geophysical Research: Planets* 112, E05S02, 1–40, doi:10.1029/2005JE002605.

McMahon, S.K., 1996. Overview of the Planetary Data System. *Planetary and Space Science* 44, 3–12.

Moore, J.M. & Howard, A.D., 2005. Large alluvial fans on Mars. *Journal of Geophysical Research* 110, E04005, 1–24, doi:10.1029/2004JE002352.

Moratto, Z.M., Broxton, M.J., Beyer, R.A., Lundy, M. & Husmann, K., 2010. Ames Stereo Pipeline, NASA's Open Source Automated Stereogrammetry Software. *Lunar and Planetary Institute Science Conference Abstracts*, 41, 41st Lunar and Planetary Science Conference, Woodlands, USA. LPI Contribution 1533, 2364.

Mustard, J.F., Murchie, S., Pelkey, S., Ehlmann, B., Milliken, R., Grant, J., Bibring, J.-P., Poulet, F., Bishop, J., Dobrea, E.N., Roach, L., Seelos, F.R., Arvidson, E., Wiseman, S., Green, R., Hash, C., Humm, D., Malaret, E., McGovern, J.A., Seelos, K., Clancy, T., Clark, R., Des Marais, D., Izenberg, N., Knudson, A., Langevin, Y., Martin, T., McGuire, P., Morris, R., Robinson, M., Roush, T., Smith, M., Swayze, G., Taylor, H., Titus, T. & Wolff, M., 2008. Hydrated silicate minerals on Mars observed by the Mars Reconnaissance Orbiter CRISM instrument. *Nature* 454, 305–309, doi: 10.1038/nature07097.

NASA Ames Research Center, 2013. *The Ames Stereo Pipeline: NASA's Open Source Automated Stereogrammetry Software. A Part of the NASA NeoGeography Toolkit. Version 2.2.2*. NASA. http://ti.arc.nasa.gov/tech/asr/intelligent-robotics/ngt/stereo/.

Neukum, G., Jaumann, R. & HRSC Co-Investigator Team, 2004. HRSC: The High Resolution Stereo Camera of Mars Express. *ESA Special Publications* SP-1240.

Nimmo, F. & Tanaka, K., 2005. Early Crustal Evolution of Mars. *Annual Review of Earth and Planetary Sciences* 33, 133–161, doi:10.1146/annurev.earth.33.092203.122637.

Parker, T.J. & Currey, D.R., 2001. Extraterrestrial coastal geomorphology. *Geomorphology* 37, 303–328.

Poulet, F., Bibring, J.-P., Mustard, J.F., Gendrin, A., Mangold, N., Langevin, Y., Arvidson, R.E., Gondet, B., Gomez, C. & Omega Team, 2005. Phyllosilicates on Mars and implications for early Martian climate. *Nature* 438, 623–627, doi:10.1038/nature04274.

Smith, D.E., Zuber, M.T., Frey, H.V., Garvin, J.B., Head, J.W., Muhleman, D.O., Pettengill, G.H., Phillips, R.J., Solomon, S.C., Zwally, H.J., Banerdt, W.B., Duxbury, T.C., Golombek, M.P., Lemoine, F.G., Neumann, G.A., Rowlands, D.D., Aharonson, O., Ford, P.G., Ivanov, A.B., Johnson, C.L., McGovern, P.J., Abshire, J.B., Afzal, R.S. & Sun, X., 2001. Mars Orbiter Laser Altimeter: Experiment summary after the first year of global mapping of Mars. *Journal of Geophysical Research* 106, 23689–23722.

Squyres, S.W., Grotzinger, J.P., Arvidson, R.E., Bell III, J.F., Calvin, W., Christensen, P.R., Clark, B.C., Crisp, J.A., Farrand, W.H., Herkenhoff, K.E., Johnson, J.R., Klingelhöfer, G., Knoll, A. H., McLennan, S.M., McSween Jr., H. Y., Morris, R.V., Rice Jr., J.W., Rieder, R. & Soderblom, L.A., 2004. In situ evidence for an ancient aqueous environment at Meridiani Planum, Mars. *Science* 306, 5702, 1709–1714, doi:10.1126/science.1104559.

Tagil, S. & Jenness, J., 2008. GIS-based automated landform classification and topographic, landcover and geologic attributes of landforms around the Yazoren Polje, Turkey. *Journal of Applied Sciences* 8, 910–921.

Webb, V.E., 2004. Putative shorelines in northern Arabia Terra, Mars. *Journal of Geophysical Research: Planets* 109, E09010, 1–12, doi: 10.1029/2003JE002205.

Webster, C.R., Mahaffy, P.R., Flesch, G.J., Niles, P.B., Jones, J.H., Leshin, L.A., Atreya, S.K., Stern, J.C., Christensen, L.E., Owen, T., Franz, H., Pepin, R.O., Steele, A. & MSL Science Team, 2013. Isotope ratios of H, C, and O in CO_2 and H_2O of the Martian atmosphere. *Science* 341(6143), 260–263.

Williams, R.M.E., Grotzinger, J.P., Dietrich, W.E., Gupta, S., Sumner, D.Y., Wiens, R.C., Mangold, N., Malin, M.C., Edgett, K.S., Maurice, S., Forni, O., Gasnault, O., Ollila, A., Newsom, H.E., Dromart, G., Palucis, M.C., Yingst, R.A., Anderson, R.B., Herkenhoff, K.E., Le Mouélic, S., Goetz, W., Madsen, M.B., Koefoed, A., Jensen, J.K., Bridges, J.C., Schwenzer, S.P., Lewis, K.W., Stack, K.M., Rubin, D., Kah, L.C., Bell, J.F., Farmer, J.D., Sullivan, R., Van Beek, T., Blaney, D.L., Pariser, O., Deen, R.G. & MSL Science Team, 2013. Martian fluvial conglomerates at Gale Crater. *Science* 340(6136), 1068–1072.

Wood, L.J., 2006. Quantitative geomorphology of the Mars Eberswalde Delta. *Geological Society of America Bulletin* 118, 557–566.

Manuscript received: 30 December 2013
Revision accepted: 20 September 2014